Biomedical Optics EXPRESS

Monitoring airway mucus flow and ciliary activity with optical coherence tomography

Amy L. Oldenburg,[1,2,*] Raghav K. Chhetri,[1] David B. Hill,[3] and Brian Button[3]

[1]*Department of Physics and Astronomy, University of North Carolina at Chapel Hill, Chapel Hill, NC 27599, USA*
[2]*Biomedical Research Imaging Center, University of North Carolina at Chapel Hill, Chapel Hill, NC 27599, USA*
[3]*Cystic Fibrosis/Pulmonary Research and Treatment Center, University of North Carolina at Chapel Hill, Chapel Hill, NC 27599, USA*
aold@physics.unc.edu

Abstract: Muco-ciliary transport in the human airway is a crucial defense mechanism for removing inhaled pathogens. Optical coherence tomography (OCT) is well-suited to monitor functional dynamics of cilia and mucus on the airway epithelium. Here we demonstrate several OCT-based methods upon an actively transporting *in vitro* bronchial epithelial model and *ex vivo* mouse trachea. We show quantitative flow imaging of optically turbid mucus, semi-quantitative analysis of the ciliary beat frequency, and functional imaging of the periciliary layer. These may translate to clinical methods for endoscopic monitoring of muco-ciliary transport in diseases such as cystic fibrosis and chronic obstructive pulmonary disease (COPD).

OCIS codes: (170.4500) Optical coherence tomography; (110.4153) Motion estimation and optical flow; (170.2655) Functional monitoring and imaging; (170.3880) Medical and biological imaging; (110.6150) Speckle imaging; (110.0113) Imaging through turbid media.

References and links

1. A. Wanner, M. Salathé, and T. G. O'Riordan, "Mucociliary clearance in the airways," Am. J. Respir. Crit. Care Med. **154**(6 Pt 1), 1868–1902 (1996).
2. J. A. Regnis, M. Robinson, D. L. Bailey, P. Cook, P. Hooper, H. K. Chan, I. Gonda, G. Bautovich, and P. T. Bye, "Mucociliary clearance in patients with cystic fibrosis and in normal subjects," Am. J. Respir. Crit. Care Med. **150**(1), 66–71 (1994).
3. G. C. Smaldone, W. M. Foster, T. G. O'Riordan, M. S. Messina, R. J. Perry, and E. G. Langenback, "Regional impairment of mucociliary clearance in chronic obstructive pulmonary disease," Chest **103**(5), 1390–1396 (1993).
4. M. R. Knowles and R. C. Boucher, "Mucus clearance as a primary innate defense mechanism for mammalian airways," J. Clin. Invest. **109**(5), 571–577 (2002).
5. M. B. Antunes and N. A. Cohen, "Mucociliary clearance--a critical upper airway host defense mechanism and methods of assessment," Curr. Opin. Allergy Clin. Immunol. **7**(1), 5–10 (2007).
6. C. Pitris, M. E. Brezinski, B. E. Bouma, G. J. Tearney, J. F. Southern, and J. G. Fujimoto, "High resolution imaging of the upper respiratory tract with optical coherence tomography: a feasibility study," Am. J. Respir. Crit. Care Med. **157**(5 Pt 1), 1640–1644 (1998).
7. H. O. Coxson, B. Quiney, D. D. Sin, L. Xing, A. M. McWilliams, J. R. Mayo, and S. Lam, "Airway wall thickness assessed using computed tomography and optical coherence tomography," Am. J. Respir. Crit. Care Med. **177**(11), 1201–1206 (2008).
8. S. Lam, B. Standish, C. Baldwin, A. McWilliams, J. leRiche, A. Gazdar, A. I. Vitkin, V. Yang, N. Ikeda, and C. MacAulay, "*In vivo* optical coherence tomography imaging of preinvasive bronchial lesions," Clin. Cancer Res. **14**(7), 2006–2011 (2008).
9. J. P. Williamson, R. A. McLaughlin, W. J. Noffsinger, A. L. James, V. A. Baker, A. Curatolo, J. J. Armstrong, A. Regli, K. L. Shepherd, G. B. Marks, D. D. Sampson, D. R. Hillman, and P. R. Eastwood, "Elastic properties of the central airways in obstructive lung diseases measured using anatomical optical coherence tomography," Am. J. Respir. Crit. Care Med. **183**(5), 612–619 (2011).
10. J. Su, J. Zhang, L. Yu, H. G Colt, M. Brenner, and Z. Chen, "Real-time swept source optical coherence tomography imaging of the human airway using a microelectromechanical system endoscope and digital signal processor," J. Biomed. Opt. **13**(3), 030506 (2008).
11. R. G. Michel, G. T. Kinasewitz, K. M. Fung, and J. I. Keddissi, "Optical coherence tomography as an adjunct to flexible bronchoscopy in the diagnosis of lung cancer: a pilot study," Chest **138**(4), 984–988 (2010).
12. K. Jeong, J. J. Turek, and D. D. Nolte, "Speckle fluctuation spectroscopy of intracellular motion in living tissue using coherence-domain digital holography," J. Biomed. Opt. **15**(3), 030514 (2010).

#168949 - $15.00 USD Received 21 May 2012; revised 6 Jul 2012; accepted 6 Jul 2012; published 1 Aug 2012

13. D. D. Nolte, R. An, J. Turek, and K. Jeong, "Holographic tissue dynamics spectroscopy," J. Biomed. Opt. **16**(8), 087004 (2011).
14. S. Jonas, D. Bhattacharya, M. K. Khokha, and M. A. Choma, "Microfluidic characterization of cilia-driven fluid flow using optical coherence tomography-based particle tracking velocimetry," Biomed. Opt. Express **2**(7), 2022–2034 (2011).
15. J. C. Hogg, F. Chu, S. Utokaparch, R. Woods, W. M. Elliott, L. Buzatu, R. M. Cherniack, R. M. Rogers, F. C. Sciurba, H. O. Coxson, and P. D. Paré, "The nature of small-airway obstruction in chronic obstructive pulmonary disease," N. Engl. J. Med. **350**(26), 2645–2653 (2004).
16. T. Aikawa, S. Shimura, H. Sasaki, M. Ebina, and T. Takishima, "Marked goblet cell hyperplasia with mucus accumulation in the airways of patients who died of severe acute asthma attack," Chest **101**(4), 916–921 (1992).
17. R. M. Shah, W. Sexauer, B. J. Ostrum, S. B. Fiel, and A. C. Friedman, "High-resolution CT in the acute exacerbation of cystic fibrosis: evaluation of acute findings, reversibility of those findings, and clinical correlation," AJR Am. J. Roentgenol. **169**(2), 375–380 (1997).
18. S. H. Donaldson, W. D. Bennett, K. L. Zeman, M. R. Knowles, R. Tarran, and R. C. Boucher, "Mucus clearance and lung function in cystic fibrosis with hypertonic saline," N. Engl. J. Med. **354**(3), 241–250 (2006).
19. L. Liu, J. A. Gardecki, S. K. Nadkarni, J. D. Toussaint, Y. Yagi, B. E. Bouma, and G. J. Tearney, "Imaging the subcellular structure of human coronary atherosclerosis using micro-optical coherence tomography," Nat. Med. **17**(8), 1010–1014 (2011).
20. B. Povazay, K. Bizheva, A. Unterhuber, B. Hermann, H. Sattmann, A. F. Fercher, W. Drexler, A. Apolonski, W. J. Wadsworth, J. C. Knight, P. S. J. Russell, M. Vetterlein, and E. Scherzer, "Submicrometer axial resolution optical coherence tomography," Opt. Lett. **27**(20), 1800–1802 (2002).
21. M. L. Fulcher, S. Gabriel, K. A. Burns, J. R. Yankaskas, and S. H. Randell, "Well-differentiated human airway epithelial cell cultures," Methods Mol. Med. **107**, 183–206 (2005).
22. J. H. Raphael, D. A. Selwyn, S. D. Mottram, J. A. Langton, and C. O'Callaghan, "Effects of 3 MAC of halothane, enflurane and isoflurane on cilia beat frequency of human nasal epithelium *in vitro*," Br. J. Anaesth. **76**(1), 116–121 (1996).
23. A. L. Oldenburg, C. M. Gallippi, F. Tsui, T. C. Nichols, K. N. Beicker, R. K. Chhetri, D. Spivak, A. Richardson, and T. H. Fischer, "Magnetic and contrast properties of labeled platelets for magnetomotive optical coherence tomography," Biophys. J. **99**(7), 2374–2383 (2010).
24. A. L. Oldenburg, V. Crecea, S. A. Rinne, and S. A. Boppart, "Phase-resolved magnetomotive OCT for imaging nanomolar concentrations of magnetic nanoparticles in tissues," Opt. Express **16**(15), 11525–11539 (2008).
25. A. L. Oldenburg and R. K. Chhetri, "Digital dispersion compensation for ultrabroad-bandwidth single-camera spectral-domain polarization-sensitive OCT," Proc. SPIE **7889**, 78891V (2011).
26. D. L. Marks, A. L. Oldenburg, J. J. Reynolds, and S. A. Boppart, "Digital algorithm for dispersion correction in optical coherence tomography for homogeneous and stratified media," Appl. Opt. **42**(2), 204–217 (2003).
27. B. White, M. Pierce, N. Nassif, B. Cense, B. Park, G. Tearney, B. Bouma, T. Chen, and J. de Boer, "*In vivo* dynamic human retinal blood flow imaging using ultra-high-speed spectral domain optical coherence tomography," Opt. Express **11**(25), 3490–3497 (2003).
28. J. A. Izatt, M. D. Kulkarni, S. Yazdanfar, J. K. Barton, and A. J. Welch, "*In vivo* bidirectional color Doppler flow imaging of picoliter blood volumes using optical coherence tomography," Opt. Lett. **22**(18), 1439–1441 (1997).
29. V. J. Srinivasan, H. Radhakrishnan, E. H. Lo, E. T. Mandeville, J. Y. Jiang, S. Barry, and A. E. Cable, "OCT methods for capillary velocimetry," Biomed. Opt. Express **3**(3), 612–629 (2012).
30. L. N. Bohs and G. E. Trahey, "A novel method for angle independent ultrasonic imaging of blood flow and tissue motion," IEEE Trans. Biomed. Eng. **38**(3), 280–286 (1991).
31. I. A. Hein and W. R. O'Brien, "Current time-domain methods for assessing tissue motion by analysis from reflected ultrasound echoes-a review," IEEE Trans. Ultrason. Ferroelectr. Freq. Control **40**(2), 84–102 (1993).
32. E. A. Swanson, J. A. Izatt, M. R. Hee, D. Huang, C. P. Lin, J. S. Schuman, C. A. Puliafito, and J. G. Fujimoto, "*In vivo* retinal imaging by optical coherence tomography," Opt. Lett. **18**(21), 1864–1866 (1993).
33. J. Schmitt, "OCT elastography: imaging microscopic deformation and strain of tissue," Opt. Express **3**(6), 199–211 (1998).
34. H. Matsui, B. R. Grubb, R. Tarran, S. H. Randell, J. T. Gatzy, C. W. Davis, and R. C. Boucher, "Evidence for periciliary liquid layer depletion, not abnormal ion composition, in the pathogenesis of cystic fibrosis airways disease," Cell **95**(7), 1005–1015 (1998).
35. S. Gueron, K. Levit-Gurevich, N. Liron, and J. J. Blum, "Cilia internal mechanism and metachronal coordination as the result of hydrodynamical coupling," Proc. Natl. Acad. Sci. U.S.A. **94**(12), 6001–6006 (1997).
36. A. B. Lansley, M. J. Sanderson, and E. R. Dirksen, "Control of the beat cycle of respiratory tract cilia by Ca^{2+} and cAMP," Am. J. Physiol. **263**(2 Pt 1), L232–L242 (1992).
37. D. B. Hill, V. Swaminathan, A. Estes, J. Cribb, E. T. O'Brien, C. W. Davis, and R. Superfine, "Force generation and dynamics of individual cilia under external loading," Biophys. J. **98**(1), 57–66 (2010).
38. Y. Zhao, Z. Chen, C. Saxer, Q. Shen, S. Xiang, J. F. de Boer, and J. S. Nelson, "Doppler standard deviation imaging for clinical monitoring of *in vivo* human skin blood flow," Opt. Lett. **25**(18), 1358–1360 (2000).
39. G. Liu, L. Chou, W. Jia, W. Qi, B. Choi, and Z. Chen, "Intensity-based modified Doppler variance algorithm: application to phase instable and phase stable optical coherence tomography systems," Opt. Express **19**(12), 11429–11440 (2011).
40. Y. Wang and R. Wang, "Autocorrelation optical coherence tomography for mapping transverse particle-flow velocity," Opt. Lett. **35**(21), 3538–3540 (2010).
41. W. M. Foster, E. Langenback, and E. H. Bergofsky, "Measurement of tracheal and bronchial mucus velocities in man: relation to lung clearance," J. Appl. Physiol. **48**(6), 965–971 (1980).

#168949 - $15.00 USD Received 21 May 2012; revised 6 Jul 2012; accepted 6 Jul 2012; published 1 Aug 2012

42. H. Matsui, S. H. Randell, S. W. Peretti, C. W. Davis, and R. C. Boucher, "Coordinated clearance of periciliary liquid and mucus from airway surfaces," J. Clin. Invest. **102**(6), 1125–1131 (1998).
43. Z. Y. Shen, M. Wang, Y. H. Ji, Y. H. He, X. S. Dai, P. Li, and H. Ma, "Transverse flow velocity quantification using optical coherence tomography with correlation," Laser Phys. Lett. **8**(4), 318–323 (2011).
44. E. Puchelle, J. M. Zahm, and D. Quemada, "Rheological properties controlling mucociliary frequency and respiratory mucus transport," Biorheology **24**(6), 557–563 (1987).
45. A. Robertson, W. Stannard, C. Passant, C. O'Callaghan, and A. Banerjee, "What effect does isoflurane have upon ciliary beat pattern: an *in vivo* study," Clin. Otolaryngol. Allied Sci. **29**(2), 157–160 (2004).
46. B. R. Manawadu, S. R. Mostow, and F. M. LaForce, "Impairment of tracheal ring ciliary activity by halothane," Anesth. Analg. **58**(6), 500–504 (1979).

1. Introduction

During respiration, humans inhale thousands of airborne pathogens per hour that are deposited onto the surface of the airways. To combat this constant influx of pathogens, the respiratory tract is lined with airway surface liquid consisting of a mucus layer and a periciliary layer (PCL) [1]. Within the PCL, cilia on the epithelium beat in a coordinated fashion to clear mucus from the airways. In diseases such as cystic fibrosis (CF) [2] and chronic obstructive pulmonary disease (COPD) [3], thickened mucus results in defective mucociliary clearance (MCC), leading to chronic lung infection and impaired pulmonary function. As such, MCC from the lung is a critical biomarker of respiratory health [4]. Currently, *in vivo* measurements of MCC are typically performed by having a patient inhale technetium particles, with clearance measured by a gamma camera [5]. This method provides the overall clearance rates across gross sections of the lung. However, this method cannot capture fine heterogeneities in MCC, or functional metrics such as the thickness of the mucus layer and the ciliary beat frequency (CBF). OCT presents the unique opportunity to accurately measure MCC, the depth of the mucus layer, and ciliary activity in the lung, providing clinicians with a more reliable measure of MCC. In this paper we describe several methods for quantifying airway functional metrics, and demonstrate them in actively transporting *in vitro* models and *ex vivo* tissues.

Since early studies using OCT to image the respiratory tract [6], the applications of OCT for *in vivo* human imaging of the airways have been growing. Some notable studies include a 44 subject study of airway wall thickness in COPD [7], a 148 subject study of pre-invasive bronchial lesions [8], a 43 subject study of airway compliance in a variety of pulmonary diseases [9], the development of a 2.2 mm diameter probe for real-time imaging in the bronchus [10], and development of an OCT probe guided by flexible bronchoscope to detect suspicious masses in the lung [11]. OCT imaging of MCC in the human airway represents a particular challenge because of the large dynamic range of time scales involved, from slow mucus flow rates to rapid ciliary beating. Recent work has demonstrated how a variety of cellular processes can be characterized by unique speckle fluctuation spectroscopic signatures [12,13]. Here we characterize, for the first time, the speckle fluctuation spectra of human airways, and show how selecting different passbands allows us to preferentially contrast mucus flow or ciliary activity within airway epithelium.

To quantify mucus transport rates, a method for tracking cilia-driven flow using particle tracking velocimetry (PTV) in OCT was recently demonstrated [14], where it was emphasized that the ability for OCT to depth-resolve flow is crucial for understanding the physiology of cilia-driven flow. However, we find that PTV is not always possible in airway mucus that is turbid and produces OCT images that are non-sparse. Importantly, people with CF, COPD, and asthma suffer from thick mucus and mucus plugging which impede pulmonary function [15–17]. In CF in particular, the ability to monitor improvements in MCC during therapeutic intervention would be beneficial [18]. To address this, here we demonstrate a cross-correlation method for quantifying flow of thick and optically turbid mucus.

Another imaging challenge is the small size of airway cilia (~7 μm in length), which would require the use of novel sub- and single-micrometer resolution OCT systems, such as those previously reported [19,20], in order to spatially resolve them. However, as we will show below, functional information on the cilia beat frequency (CBF) can still be obtained with a more moderate axial resolution of ~3 μm, which is sufficient to resolve the PCL.

#168949 - $15.00 USD Received 21 May 2012; revised 6 Jul 2012; accepted 6 Jul 2012; published 1 Aug 2012

Overall, this paper describes OCT-based methods for quantifying mucus flow, CBF, and imaging ciliary activity, which are demonstrated on both *in vitro* and *ex vivo* airway epithelium models.

2. Methods

2.1. In vitro and ex vivo airway models

Our *in vitro* model for airway epithelium consists of primary, normal human bronchial epithelial (hBE) cells that are cultured on a porous membrane (Fig. 1). This model recapitulates several important features of the human airway epithelium [21]. As cells develop over several weeks, they become polarized and form a contiguous epithelium, acting to exclude liquid media from their apical surface so that they reside at an air-liquid interface. Also, the hBE cells secrete mucus, which accumulates over time in culture. Importantly, hBE cells grow cilia at the apical surface, which beat in a coordinated fashion and actively transport mucus. Because these cells are cultured in a circular horizontal culture dish, unlike *in vivo*, they tend to transport accumulated mucus in a rotational, hurricane-like, pattern.

In this study, hBE cells were cultured on 0.4 mm pore size Millicells (Millipore, Billerica, MA) coated with collagen and maintained in air-liquid interface media (UNC Tissue Core) as described previously [21]. Cultures were examined after 6 weeks, when the hBE cells were confluent, had fully developed cilia, and were able to transport mucus. Hurricane cultures were allowed to accumulate mucus over a 48 hr period prior to imaging. Mucus hurricane

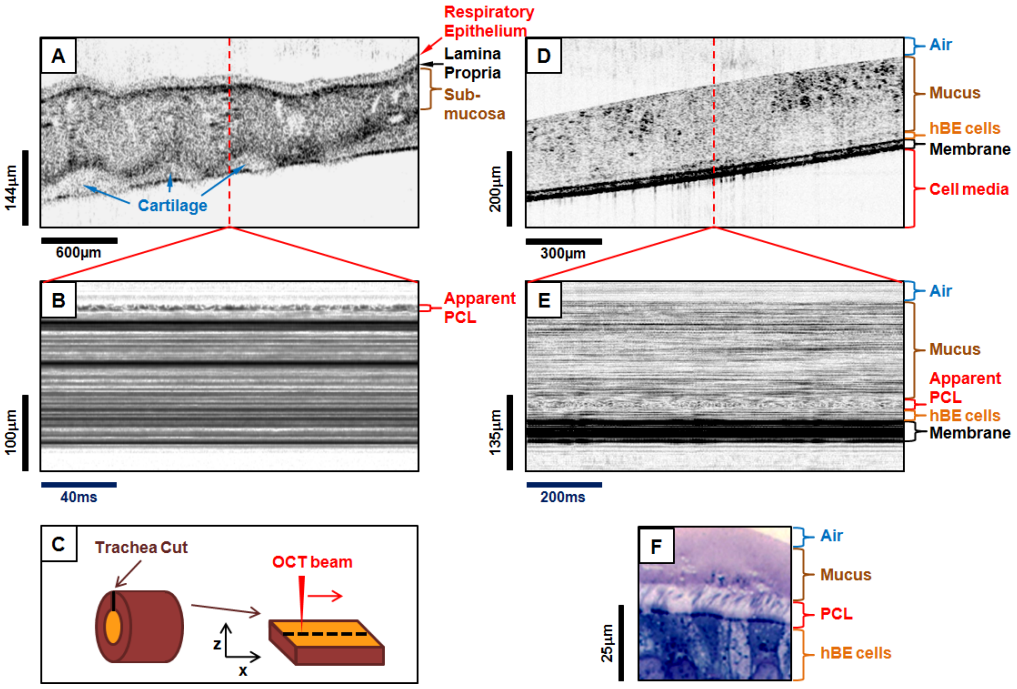

Fig. 1. Representative OCT images of airway models. (a) B-mode (*x*-*z*) OCT of *ex vivo* mouse trachea. (b) M-mode (*time*-*z*) OCT of *ex vivo* mouse trachea associated with panel (a). The apparent location of the periciliary layer (PCL) is indicated by regions of rapid speckle fluctuation. (c) Diagram of geometry used for opening and subsequently imaging the mouse trachea. (d) B-mode OCT of *in vitro* hBE model with thick mucus at an air-liquid interface. The porous membrane is highly optically scattering, while the hBE cells are observed as a more weakly scattering layer immediately above the membrane. The thick mucus layer above the hBE cells is also optically scattering due to cellular detritus. (e) M-mode OCT of the *in vitro* model associated with panel (d). The apparent PCL is located immediately above the hBE cell layer, as expected. (f) Representative histology section of an *in vitro* hBE culture showing the detailed structure of the epithelium; this culture exhibited a thinner mucus layer than the one depicted in (d) and (e).

#168949 - $15.00 USD Received 21 May 2012; revised 6 Jul 2012; accepted 6 Jul 2012; published 1 Aug 2012

imaging was performed both with OCT (described below), and, for validation, on an Olympus IX-71 Inverted Microscope operating in standard brightfield mode, with both 4 × and 10 × objectives. Microscopy image sequences were collected using a JAI CM-030GE grey-scale camera at 90 fps and sampled over 1215 × 914 μm into 656 × 494 pixels in $x \times y$, respectively. For histology, cells were fixed with osmium tetraoxide in perfluorocarbon, Epon-embedded, and stained with Richardson's.

For *ex vivo* tissues, tracheas from 3 mice (C57BL/6) were obtained from freshly sacrificed mice and kept in saline before OCT imaging. All mice were handled according to approved protocols at the Institutional Animal Care and Use Committee (IACUC) at the University of North Carolina at Chapel Hill. Two tracheas were sliced axially and opened for imaging perpendicular to the luminal surface (as shown in Fig. 1(c)), while the third trachea was kept intact for imaging of both luminal and basal surfaces (OCT beam nearly parallel to these surfaces).

Both *in vitro* and *ex vivo* models were imaged before and after isoflurane treatment, which is known to slow ciliary activity [22]. This was performed by incubating the cells or tissues with ~20% isoflurane for 5 minutes, rinsing with saline, and immediately imaging.

2.2. OCT system hardware and data acquisition

The spectral domain OCT system used in this study has been described in detail previously [23]. Briefly, a Ti:sapphire laser (KMLabs, Inc.) provided light centered at 810 nm with a 3 dB bandwidth of 125 nm, corresponding to a coherence length of 2 μm in tissue. The light was directed into a free space Michelson interferometer with 10 mW of optical power incident upon the sample and imaging optics providing a transverse resolution of 12 μm and a confocal parameter of 0.28 mm. The output of the interferometer was directed into a spectrometer to sample the spectral interferogram into 2048 pixels of a line scan camera (Dalsa Piranha 2). OCT images were obtained by Fourier transformation of the spectral interferogram after processing steps including reference spectrum subtraction [24] and digital dispersion compensation [25,26]. The signal-to-noise ratio of this system was typically >95 dB.

B-mode OCT was performed for mucus flow studies and speckle fluctuation contrast of the PCL. Images were collected in *x-z* (transverse × axial) over (1–3) × 1.5 mm into (150–1000) × 1024 pixels, respectively. The camera linerate was set to either 5 or 10 kHz for collection of 100 frames in a time series, at adjustable frame rates spanning from 0.82 fps to 40 fps. M-mode OCT was also performed for cilia beat rate analysis with the same parameters as in B-mode except the *x* dimension was not scanned, and only 10 sequential frames were recorded.

2.3. Mucus flow imaging by cross-correlation

Imaging airway mucus flow is challenging for several reasons. Mucus flow is predominantly transverse to the OCT beam axis in typical imaging geometries, but transverse flows are not possible to measure with traditional Doppler OCT techniques [27,28]. New Doppler methods for quantifying both transverse and axial flows have been developed for hemodynamic imaging [29], but are affected by the distribution of sizes and anisotropy of the scattering particles within the flow volume, which may be difficult to control in airway mucus. Furthermore, mucus flow velocities are typically 2 orders of magnitude smaller than blood flow, with flow velocities typically ranging from 10–60 μm/s. This longer time scale makes it more difficult to maintain phase stability needed for Doppler OCT while particles traverse the imaging beam. On the other hand, mucus flow can be effectively frozen by imaging at moderate frame rates in the 10s of Hz, suggesting the use of PTV, such as recently reported for studying cilia-driven flow [14]. However, in that study, the fluids were optically clear and tracer particles were added. We find that mucus that has accumulated in hBE cultures contains a large amount of cellular detritus, making it optically turbid with developed speckles in the OCT image, and thus does not fit the requirement of sparse imaging needed for PTV.

#168949 - $15.00 USD Received 21 May 2012; revised 6 Jul 2012; accepted 6 Jul 2012; published 1 Aug 2012

Importantly, people suffering from many respiratory diseases have characteristically thick mucus.

Given these challenges, we employed a normalized, 2D cross-correlation for speckle tracking. These types of methods were originally developed for motion tracking in ultrasonic imaging [30,31], and have been previously employed in OCT for compensation of motion artifacts [32] and for tracking elastic deformation [33]. Given a point (x_0, z_0) around which we wish to compute the velocity, we first obtained a normalized cross-correlation between two images in the time series, I_1 and I_2, separated by Δt_{12} in time, as follows:

$$\rho(x',z') = \frac{\int_{z_0-Z/2}^{z_0+Z/2} dz \int_{x_0-X/2}^{x_0+X/2} dx \;\; I_1(x,z) I_2(x-x', z-z')}{\left[\left(\int_{z_0-Z/2}^{z_0+Z/2} dz \int_{x_0-X/2}^{x_0+X/2} dx \;\; I_1^2(x,z) \right) \left(\int_{z_0-Z/2}^{z_0+Z/2} dz \int_{x_0-X/2}^{x_0+X/2} dx \;\; I_2^2(x,z) \right) \right]^{1/2}}, \quad (1)$$

where X and Z are the window sizes and the correlation $\rho(x',z')$ is computed over $\left(-\Delta x_{\max} < x' < \Delta x_{\max}\right)$ and $\left(-\Delta z_{\max} < z' < \Delta z_{\max}\right)$, where $\Delta x_{\max}$ and $\Delta z_{\max}$ are the maximum displacement sizes. We then found the values of x' and z' at which $\rho(x',z')$ was at a maximum, and determined the velocity components $v_x = (x_0\text{-}x')/\Delta t_{12}$ and $v_z = (z_0\text{-}z')/\Delta t_{12}$. v_x and v_z were then obtained at all desired values of (x_0, z_0) to generate a velocity map.

Balancing the added time of computation against increasing the available dynamic range in velocity, we chose window sizes of $X = 30$ and $Z = 10$ pixels, maximum displacement sizes of $\Delta x_{\max} = 8$ and $\Delta z_{\max} = 5$ pixels, and sampled x_0 and z_0 on a 5 × 5 pixel mesh within the image. We omitted any (x_0, z_0) points where the root-mean-squared (RMS) pixel intensities summed over the window (the denominator in Eq. (1)) was less than a threshold value. Because mucus flow is approximately in a steady-state in the *in vitro* models, we reduced noise by obtaining the median values of v_x and v_z over time intervals Δt_{ij} across the entire time series (every 5–10 frames, or 0.5–1s intervals, over 100 frames, or 10s). It was important to adjust the time interval so that the maximum displacement would be close to but less than $\Delta x_{\max}$ or $\Delta z_{\max}$ in order to maximize the dynamic range. We also rotated the reference frame to align with that of the epithelial cell layer, which was slightly tilted with respect to the incident beam. The resulting v_x and v_z maps were 2 × 2 mean filtered and visualized in a hue-saturation-value (HSV) color map by assigning hue to velocity and saturation and value to RMS pixel intensity.

We applied the same method to *x*-*y* microscopy images collected for flow validation, with settings $\Delta t_{ij} = 0.55$s, $X = 20$ and $Y = 20$ pixels, $\Delta x_{\max} = 5$ and $\Delta y_{\max} = 13$ pixels, and otherwise the same settings as for OCT. Test image sets were generated from both OCT and microscopy images, where each frame was stepped a known displacement over a simulated time series. Velocities extracted by cross-correlation were confirmed to match the simulated velocities.

2.4. Ciliary beat rate quantification by Fourier analysis

With some exceptions [19,20], most OCT systems currently do not offer the resolution needed to spatially resolve individual airway cilia. However, our OCT system axial resolution of ~3 μm is, in most cases, sufficient to resolve the PCL within the airway surface liquid [34], while our transverse spot size of ~12 μm covers ~12 hBE cells and ~2000 individual cilia. Despite this limitation, we expect that the speckle fluctuation arising from the movement of an ensemble of sub-resolution cilia can be related to the ciliary beat frequency (CBF), for the following reasons. It is known that neighboring cilia tend to coordinate into metachronal patterns, *i.e.*, sharing the same CBF with a constant phase difference [35]. The ciliary beat motion has a complicated shape (Fig. 2(a)) but is periodic with a frequency of typically 5 Hz at room temperature and 10 Hz at 37°C for healthy airway epithelium [36]. The speckle pattern in OCT arises from interferences between sub-resolution light scatterers, such as cilia.

#168949 - $15.00 USD Received 21 May 2012; revised 6 Jul 2012; accepted 6 Jul 2012; published 1 Aug 2012

During the cilia beat cycle we would expect these interferences to change in a highly complicated way (Fig. 2(b)), however, fundamentally this pattern should be time-periodic. As such, we would expect the Fourier spectrum of speckle fluctuations from cilia to have peaks at the CBF and its harmonics. In practice, we find that such peaks cannot be observed and are blurred together over a bandwidth several times that of the CBF. This is possibly due to overlying mucus motion changing the light beam refraction at the air-liquid interface, mucus scattering within the PCL, or creep in the system causing phase instability on this 100–200 ms time scale.

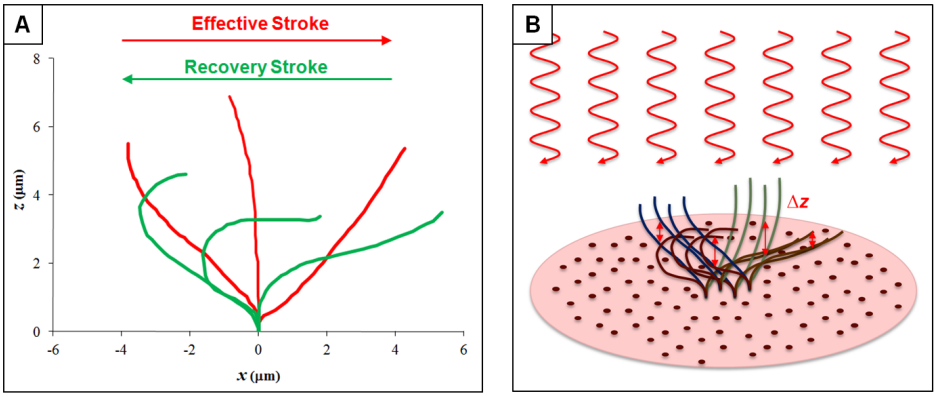

Fig. 2. (a) Diagram of cilia beat pattern during the effective stroke (red) and the recovery stroke (green) [37]. (b) Cartoon illustrating dynamic light scattering from cilia during OCT imaging. Hundreds of cilia are simultaneously illuminated by the OCT beam. The coordinated beat pattern of a few cilia are illustrated, showing how the relative axial spacing between cilia (Δz) rapidly changes during one beat cycle. The OCT signal fluctuates when Δz changes by $\lambda/2 \approx 400$ nm. This is why we expect to observe many fluctuations during a single beat cycle, giving rise to an apparent fluctuation rate many times greater than the CBF.

Despite the lack of a clear CBF spectral peak, we realized that, in the assumption that the beat motion pattern remains the same when the CBF increases or decreases, (*i.e.*, the OCT amplitude is an arbitrary, time-harmonic function that does not change pattern when the cilia speed up or slow down), one would expect the Fourier spectrum to linearly expand or contract, respectively. Mathematically one might write this as

$$\left|\mathcal{F}\left\{I\left(\omega_C t\right)\right\}\right|^2 = S\left(\frac{\omega}{\omega_C}\right) + S_{DC}\delta\left(\omega\right) + \tilde{\sigma} \qquad (2)$$

where I is the arbitrary, time-harmonic speckle amplitude arising from cilia with a characteristic CBF of ω_C, S is the power spectral density for $\omega > 0$, S_{DC} is the DC offset (δ is the Kronecker delta function), $\tilde{\sigma}$ accounts for additive white noise (such as shot noise), and negative frequencies are omitted for convenience. For noisy data, one robust method for determining the relative scale of the spectrum S is to compute its median ω_m, that is, the frequency that evenly divides the area under the power spectrum curve. According to (2), we see that ω_m is linearly proportional to ω_C, providing a relative measure of the CBF.

This method was implemented by obtaining the power spectral density S at each depth within an M-mode OCT scan and spatially averaging spectra over 3 pixels. The white noise, $\tilde{\sigma}$, was estimated as the average over the 1.5-2.5 kHz band (2.5 kHz being the Nyquist frequency); the exact choice of the lower limit of this band between 1 and 2 kHz had little effect on our results (<5%). After subtraction of the DC term and the white noise, the median ω_m was computed. Visual inspection of each image was used to determine an 8 pixel PCL region, and the maximum value of ω_m within this region was recorded for each of 10 frames collected at each of 2-3 independent positions for each sample (*in vitro* and *ex vivo*) both before and after isoflurane treatment. For the purposes of display only, ω_m was thresholded to omit rows below a minimum light scattering intensity.

#168949 - $15.00 USD Received 21 May 2012; revised 6 Jul 2012; accepted 6 Jul 2012; published 1 Aug 2012

2.5. Speckle fluctuation contrast for PCL imaging

In order to extend the 1D method above to 2D OCT imaging of the PCL, we note that high frame rates (ω_m >100 Hz) would be needed to directly capture the speckle fluctuations arising from ciliary activity. However, taking cues from OCT angiography where blood flow is often too rapid to directly capture [38], we can semi-quantitatively image ciliary activity by computing the standard deviation (or variance) of the speckle fluctuations. In our experiments, we find that phase is not generally stable, and we instead compute the variance of the OCT amplitude, a method which was recently shown to give comparable results to phase variance methods for blood flow imaging [39].

Interestingly, airway epithelium dynamics occur over a wide range of time scales, from slow mucus transport to fast ciliary beating, and so it is important to define the frequency band in which variance calculations are performed. We note that, using a discrete version of Parseval's theorem, the variance of a time series x that is sampled at intervals of Δt over a total time $T = (N\text{-}1)\Delta t$ is directly proportional to the power spectral density of x, $|X|^2$, integrated over a frequency band bounded by the spectral resolution, $\Delta f = 1/T$, and the Nyquist frequency, $f_{Nyq} = 1/(2\Delta t)$, as follows:

$$\begin{aligned}\sigma^2 &= \frac{1}{N}\sum_{n=0}^{N-1}\left|x\left(n\Delta t\right)\right|^2 - \left(\frac{1}{N}\sum_{n=0}^{N-1}x\left(n\Delta t\right)\right)^2 \\ &= \frac{1}{N^2}\sum_{k=0}^{N-1}\left|X\left(k\Delta f\right)\right|^2 - \frac{1}{N^2}\left|X\left(0\right)\right|^2 \\ &= \frac{1}{N^2}\sum_{k=1}^{N-1}\left|X\left(k\Delta f\right)\right|^2\end{aligned} \tag{3}$$

Using this relation, one can tailor the time scale of interest to match the imaging target by the choice of Δt and T. This is also a computationally efficient method in comparison to direct Fourier analysis, which is important when collecting 2- and 3-D imaging data.

We implemented this method by analyzing B-mode OCT time series collected at variable frame rates from 0.82–40 fps. The Nyquist frequency could be further reduced from that dictated by the sampling rate by skipping frames in the series, and Δf was adjusted by choosing how many images of the series to include in the analysis. The standard deviation σ was computed for each pixel across the time series, and was normalized by the shot noise estimated as the square root of the mean value in each pixel. Mean filtering of this signal was performed in 4 × 4 pixel windows. Using this method, we processed images of the *in vitro* hurricane hBE model and *ex vivo* mouse trachea into 3 frequency bands spanning nearly 3 decades.

3. Results and discussion

3.1. Mucus flow imaging

We studied an *in vitro* hBE culture exhibiting mucociliary transport of thick (~100-250 μm) mucus. Using light microscopy, we found that the transverse mucus motion was in a circular, hurricane-like pattern, consistent with previous observations in these types of cultures [21]. B-mode OCT imaging and quantitative flow analysis was performed in cross-sectional slices moving across the center of the hurricane. A representative data set obtained near the periphery of the hurricane is shown in Fig. 3. The real-time video suggests mucus motion predominantly parallel to the epithelial surface to the right (positive x direction). Also, one can observe a more rapid speckle decorrelation rate near both edges of the image. The computed flow maps corroborate these observations, where the velocity is largely homogeneous in the positive x direction, except near the edges where high variance is observed due to the rapid decorrelation. This decorrelation is likely due to the component of mucus motion through the image plane (v_y), which is expected to be greater near the edges

#168949 - $15.00 USD Received 21 May 2012; revised 6 Jul 2012; accepted 6 Jul 2012; published 1 Aug 2012

than in the center of the hurricane. This effect dictates a tradeoff in the choice of frame rate, as sufficiently high frame rate is needed to capture speckles in regions with a high v_y component, while sufficiently low frame rate is needed to allow for speckles to move a number of pixels in the x-z plane order to minimize digitization noise in the velocity measurement. In practice, we find the optimum frame rates to lie between 1–2 fps. It may be possible, in future work, to quantify v_y based upon this loss of correlation using a previously described method [40]; in this case, careful calibration would be needed to account for the beam divergence over the large imaging depth range needed to assess thick mucus.

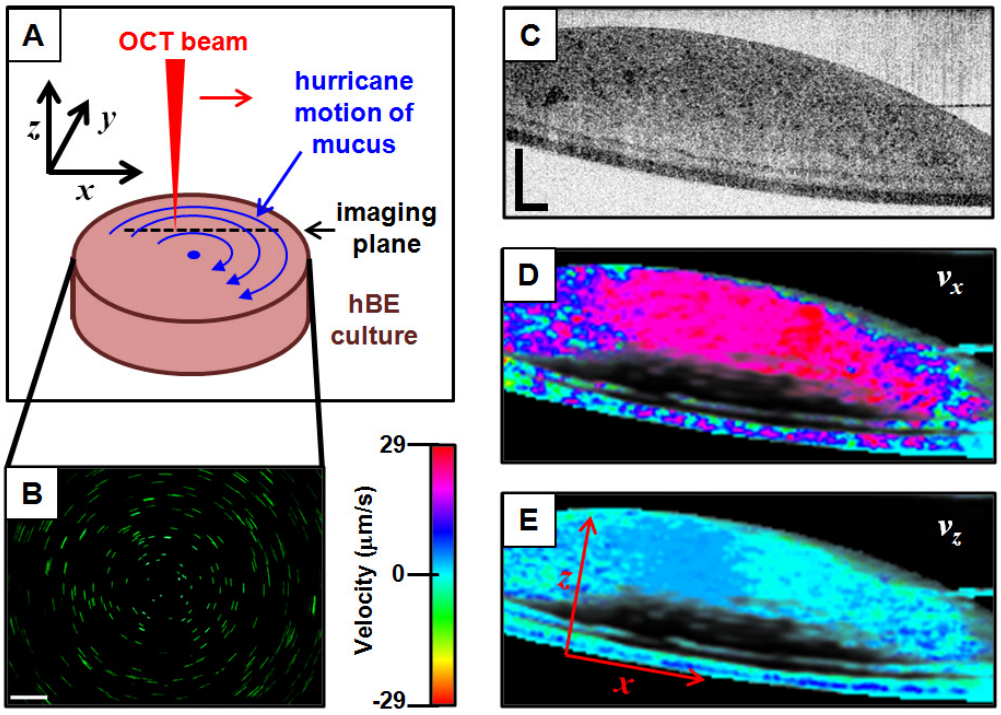

Fig. 3. Depth-resolved mucus flow imaging of an *in vitro* hBE culture with hurricane-like mucus motion. (a) Cartoon illustrating the OCT image plane off-center from the hurricane. (b) Microscopy (x-y) of 1 μm fluorescent beads trapped in mucus in an hBE culture exhibiting hurricane motion, 2 second exposure. (c) Video comprised of a B-mode (x-z) OCT time series at 2 × real time (Media 1). (d) Corresponding transverse velocity map, v_x, computed using cross-correlation. (e) Axial velocity map, v_z. All scale bars are 200 μm.

We note that OCT can provide new information about the axial component of velocity, v_z, and the depth dependence of v_x during MCC. Here we find that v_x appears to be constant in z except near the air-liquid interface; the surface effect may be an artifact of more rapid decorrelation at the interface due to changes in surface height. The homogeneous depth profile of v_x is consistent with the view that mucus travels as a slab. In comparison, v_z is not significantly different from zero. It will be interesting in future work to learn whether mucus flow in living, breathing organisms is depth-dependent due to shear forces from air flow, which may lead to better models of muco-ciliary transport.

In order to validate flow quantification by OCT, we compared the depth-averaged v_x to the components of flow $v_{x'}$ and $v_{y'}$ obtained by light microscopy; orientation was not maintained between the experiments so the axes may be different. The results are summarized in Fig. 4. For OCT, the depth-averaged v_x was computed within the mucus layer for B-mode images across a 2.7 mm × 3.0 mm (x-y) area of the hurricane. A clear transition from negatively-directed flow to positively-directed flow is seen as the B-mode slice is moved across the center of the hurricane, with values that ranged from −34 to + 35 μm/s. Microscopy was

#168949 - $15.00 USD Received 21 May 2012; revised 6 Jul 2012; accepted 6 Jul 2012; published 1 Aug 2012

performed in the same culture immediately after OCT imaging within a 0.9 mm × 1.2 mm window, resulting in a similar transition in flow direction across the center of the hurricane, with values ranging from –41 to + 29 μm/s. As a point of reference, human mucus velocity has previously been measured to be 40 μm/s in the main bronchi and 92 μm/s in the trachea in healthy subjects [41].

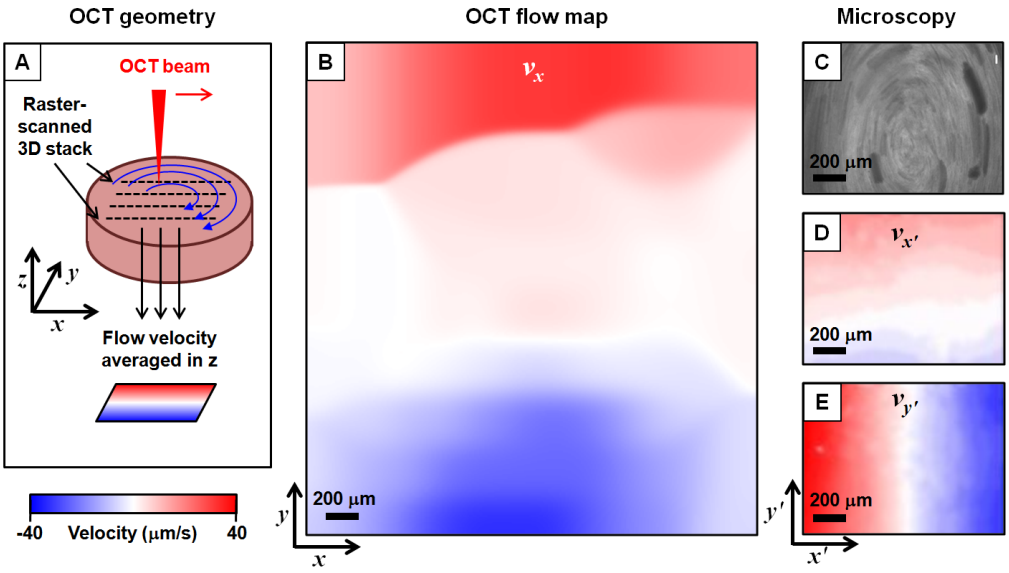

Fig. 4. Transverse mucus flow imaging of an *in vitro* hBE culture with hurricane-like motion. (a) Cartoon illustrating the OCT imaging scan pattern across the hurricane. (b) The depth-averaged velocity v_x obtained by OCT, mapped across the *x*-*y* surface of the culture, shows the reversal of flow direction across the eye of the hurricane. (c) Maximum intensity projection of a time series of microscopy images of the same hurricane. (d) and (e) Velocity components $v_{x'}$ and $v_{y'}$ obtained by microscopy, respectively. The same velocity and spatial scales are used in (b), (d), and (e).

While the OCT data was obtained over a larger area than the microscopy data, it is relevant to compare the velocity gradient across the hurricane. We find that the velocity gradient by microscopy was significantly asymmetric, with values of 25 and 61 μm s^{-1}/mm for $\partial v_{x'}/\partial y'$ and $\partial v_{y'}/\partial x'$, respectively. At the same time, we noted an elongated physical appearance to the hurricane. In comparison, the velocity gradient $\partial v_x/\partial y$ by OCT was 23 μm s^{-1}/mm, which is consistent with the slow axis observed in microscopy. Previous measures of flow in these hurricane models was reported in [42], where a similar range of velocities and a velocity gradient of ~77 μm s^{-1}/mm was observed. Future improvements to our OCT system may provide 3D imaging at sufficient frame rates to enable quantification of all mucus velocity components simultaneously. Alternately, rapid scanning of slightly offset B-mode planes could provide the v_y component locally, as demonstrated previously in phantoms [43].

3.2. Ciliary beat rate

Another important parameter is the ciliary beat frequency (CBF), because it regulates the rate of mucus clearance [44]. In order to modulate CBF in a controlled study, we used a high dose of a gaseous anesthetic, which is expected to slow the cilia [22,45,46]. As an independent measure, we first used light microscopy to monitor the effect of 20% isoflurane added to separate hBE cultures. We found that CBF dropped from an initial value of 5.2 ± 0.5 Hz to a value indistinguishable from zero in less than 5 minutes (n = 3). After extensive washing of the isoflurane, the CBF recovered to 3.7 ± 0.9 Hz, suggesting that hBE cells remain viable after isoflurane treatment. For study with OCT, we evaluated hBE cultures that had been cleared of mucus, and healthy *ex vivo* mouse trachea with only a thin, transparent mucus

#168949 - $15.00 USD Received 21 May 2012; revised 6 Jul 2012; accepted 6 Jul 2012; published 1 Aug 2012

layer, in order to directly measure the speckle fluctuations from the cilia. To validate that the median frequency, ω_m, of the speckle power spectrum is correlated with ciliary activity, we performed M-mode OCT on these models before and after 20% isoflurane.

Representative OCT data is displayed in Fig. 5. Visual inspection of the M-mode images reveals rapid speckle fluctuation within the topmost light scattering layer, which is where the PCL is expected to be located. The associated Fourier spectra versus depth reveal a strong, broadband response within this layer in comparison to the cells below. It is important to note that we also expect some motion of the basal body, where the cilia are attached, and as such, the apparent layer of high fluctuation may include some of this region beneath the actual PCL. Induced motion of mucus immediately above the PCL may also exhibit rapid speckle fluctuations. As such, our following discussion on the "apparent" PCL should be understood to include these layers, in addition to the true PCL.

Computation of ω_m versus depth reveals a peak within the PCL of ~100–120 Hz, which is many times larger than the actual CBF, as expected based on the discussion in 2.4 above. Interestingly, the full width at half maximum of this peak is approximately 7.4 ± 1.5 μm in

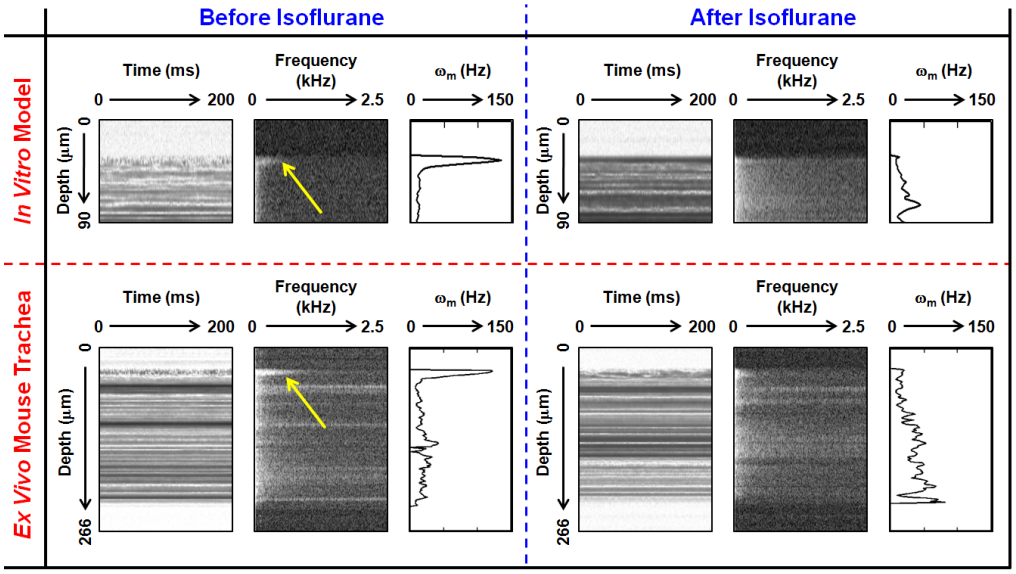

Fig. 5. Representative beat frequency analyses for *in vitro* and *ex vivo* models cleared of mucus. Results are shown before and after isoflurane treatment to slow cilia beating, from M-mode images (left images) to corresponding Fourier spectra (middle images) to median frequency ω_m (right plots). Yellow arrows indicate the depth position of the apparent PCL before isoflurane treatment; after treatment the activity is dramatically slowed within the PCL.

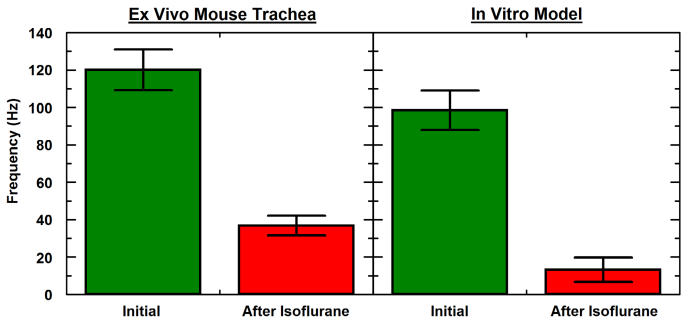

Fig. 6. Peak median frequency ω_m within the PCL for *ex vivo* and *in vivo* airways before and after isoflurane treatment. Mean and standard deviation were evaluated over 10 images each at 2-3 independent locations per sample.

#168949 - $15.00 USD Received 21 May 2012; revised 6 Jul 2012; accepted 6 Jul 2012; published 1 Aug 2012

depth, consistent with the known PCL thickness [34]. As expected, we found that ω_m diminished significantly after the application of isoflurane, to a value of ~10–40 Hz for both *ex vivo* and *in vitro* models, suggesting that ω_m scales proportionally with ciliary activity. The statistical results of the ω_m measurements are summarized in Fig. 6. Importantly, while our OCT system axial resolution (3 μm) is sufficient to resolve the PCL as a whole, we can detect changes in the ciliary activity without spatially resolving individual cilia.

3.3. PCL imaging using speckle fluctuation contrast

The results above provide a basis for producing images that selectively contrast ciliary activity, enabling identification of the PCL. The standard deviation contrast method described in 2.5 was applied first to clean hBE cultures (with no mucus), as shown in Fig. 7. In some places, hBE cells have grown in multiple layers, and ciliary activity on the borders of each

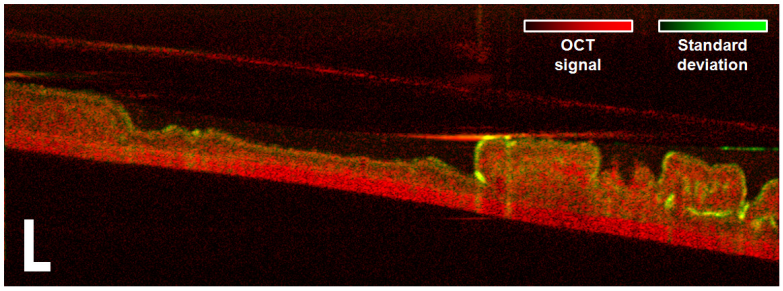

Fig. 7. Dynamic OCT imaging of *in vitro* hBE model with clear mucus using speckle fluctuation contrast in the 0.1–1 Hz band. High standard deviation at the borders of the hBE cells indicates ciliary activity. Lower left scale bars are 100μm.

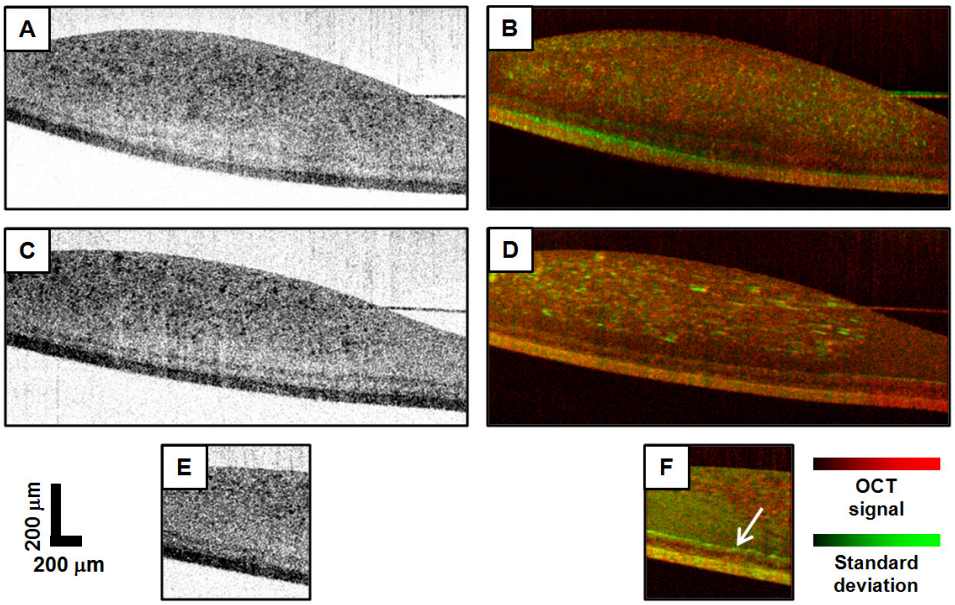

Fig. 8. Dynamic OCT imaging of an *in vitro* hBE model at varying time scales spanning 3 decades. (a) Video at 10 × real time (Media 2). (b) Standard deviation image in the 0.02–0.2 Hz band. On these long time scales mucus transport is rapid, and high variance is seen throughout the mucus. (c) Video at 1 × real time (Media 3). (d) Standard deviation image in the 0.4–5 Hz band. At these intermediate time scales we observe particle tracks from scatterers within the mucus. (e) Video at 0.2 × real time (Media 4). (f) Standard deviation image in the 3.3–17 Hz band. At these short time scales mucus transport appears frozen, and ciliary activity within the PCL becomes more evident, as indicated by the white arrow.

#168949 - $15.00 USD Received 21 May 2012; revised 6 Jul 2012; accepted 6 Jul 2012; published 1 Aug 2012

cell can be observed as regions of high speckle fluctuation. Next, dynamic imaging of hBE cultures with thick, turbid mucus was performed (Fig. 8). In this case, we observe high speckle fluctuation from mucus in frequency bands up to several Hz, including particle tracks observed particularly in the middle, 0.4-5 Hz band (Fig. 8(d)). In some sense, the optimum frame rate for mucus flow imaging (section 3.1) is within this frequency band, as it allows for speckle tracking within the mucus by cross-correlation. At the highest frequencies, however, mucus transport appears frozen, as shown in Media 4, and the ciliary activity becomes more prominent. Because PCL speckle fluctuation rates exceed 100 Hz for healthy epithelium (as shown in 3.2), we might expect even higher frame rates to provide even greater contrast between mucus and PCL.

We also performed dynamic imaging of *ex vivo* mouse trachea. To verify that the speckle fluctuation is specific to ciliated cell surfaces, and not an artifact of a cell-liquid interface, we first imaged a tracheal tube that was on-end (Fig. 9), where the outer tracheal surface is not expected to be ciliated, and the inner surface is. As expected, broad regions of high speckle fluctuation are observed only on the inner tube surfaces, corresponding to ciliary activity. Next, we imaged the along the inner tracheal surface of a tube that had been cut open axially (Fig. 9(e)), where we observed that the ciliary activity is patchy, consistent with microscopy observations of patchy ciliation. In Fig. 10, we show how imaging of the tracheal surface varies with the choice of speckle fluctuation frequency band. Because the mucus was transparent, very little interference was observed, and excellent visualization of the PCL was provided at all 3 time scales, ranging from 0.02Hz – 20Hz. Associated videos illustrate the ciliary activity within different these time scales.

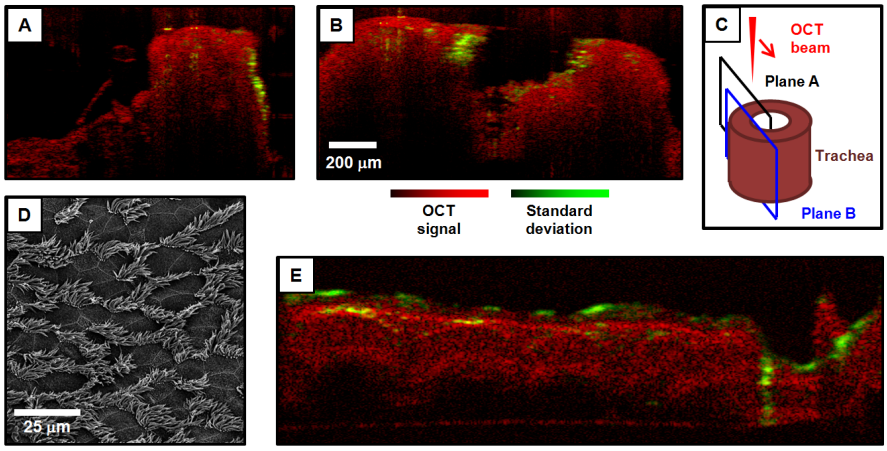

Fig. 9. Dynamic OCT of *ex vivo* trachea using speckle fluctuation contrast in the 0.1–1 Hz band. (a) Image in plane A where the luminal surface is the rightmost vertical surface. (b) Image in plane B with luminal surfaces in the center. (c) Cartoon diagram of imaging geometry. In both (a) and (b), luminal (mucosal; ciliated) tissue surfaces have high standard deviation, in comparison to serosal (non-ciliated) tissue surfaces. (d) Scanning electron microscopy of mouse trachea showing characteristic patchiness of ciliation. (e) Image of mouse trachea luminal side up (according to diagram of Fig. 1(c)), showing patchy regions of rapid fluctuation corresponding to ciliary activity. Panels (a), (b), and (e) have the same scale.

#168949 - $15.00 USD Received 21 May 2012; revised 6 Jul 2012; accepted 6 Jul 2012; published 1 Aug 2012

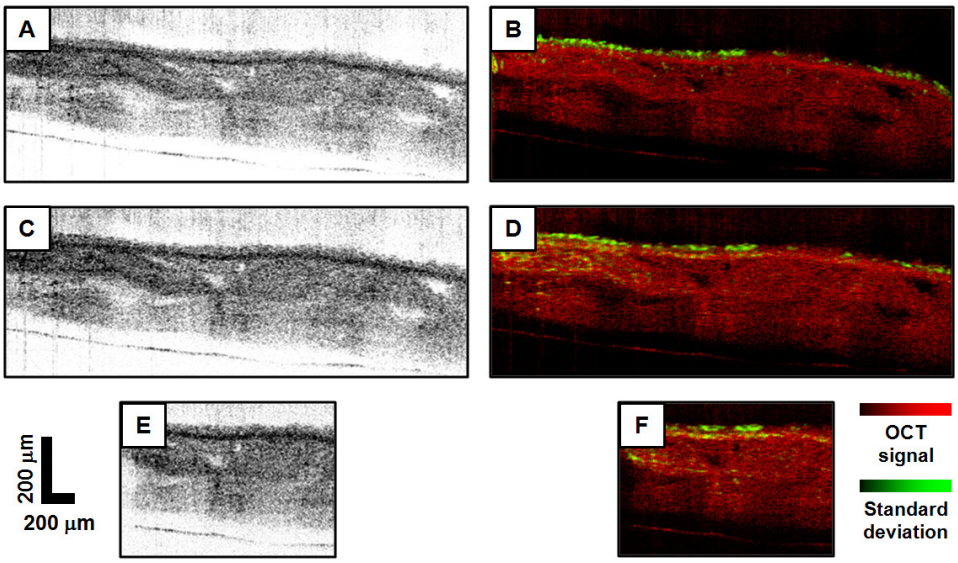

Fig. 10. Dynamic OCT imaging of cut open *ex vivo* mouse trachea (imaging geometry of Fig. 1(c)) at varying time scales spanning 3 decades. (a) Video at 10 × real time (Media 5). (b) Standard deviation image in the 0.02–0.2 Hz band. (c) Video at 1 × real time (Media 6). (d) Standard deviation image in the 0.2–2.5 Hz band. (e) Video at 0.2 × real time (Media 7). (f) Standard deviation image in the 2–20 Hz band. Because this healthy mouse lacked a thick mucus layer, the ciliary activity is highly contrasted at all time scales.

4. Conclusion

In summary, we described several methods for studying MCC in an *in vitro* human airway model and *ex vivo* mouse tracheas, including direct measurements of mucus flow using cross-correlation, indirect measurements of cilia beat frequency through a proportional parameter given by the median frequency of the power spectrum, and qualitative imaging of the PCL using variance-based contrast. We also found that ciliary activity could still be visualized underneath a thick and turbid mucus layer by choice of a sufficiently high frequency band for variance contrast (>3.3 Hz).

In addition, we measured the apparent thickness of the PCL by Fourier analysis of speckle fluctuations, and found that it was well-matched to the known thickness of PCL in healthy epithelium [34]. While future work is needed to determine whether OCT can monitor changes in PCL thickness, this ability would be clinically useful as PCL depletion is indicated in the pathogenesis of cystic fibrosis. These methods constitute a toolkit for understanding MCC in the human respiratory system, and can potentially provide new data about mucus thickness, depth-resolved flow, and ciliary activity, even in airways with thick mucus.

The ability to translate these methods to clinical imaging depends upon several factors. Patient motion and respiration will invariably cause motion artifacts on moderate (~1 Hz) time scales that may be alleviated by motion tracking methods already used in retinal imaging [32]. For diseases where access to lower airways is desired, the development of catheters with sufficiently small diameter is technically challenging, although several groups have already made progress in this area [7,8,10,11]. In terms of resolution, in our experiments, the cilia were not spatially resolved, which relaxes requirements on beam focusing needed in endoscopic systems. Fundamentally, the ability to depth-resolve MCC provides new insight in respiratory diseases, and may lead to better methods for treatment monitoring.

Acknowledgments

We acknowledge Tyler S. Ralston at Lawrence Livermore National Laboratory for technical assistance. Support for this work came from grants from the Cystic Fibrosis Foundation CFFT

BUTTON07XX0 (Button, PI), NIH 1R01HL092964 (Boucher, PI), NIH 2R01HL07546 (Superfine, PI), NFS DMS 1100281 (Hill, PI), the Cystic Fibrosis Foundation HILL0810 (Hill, PI), and startup funds from UNC Chapel Hill (Oldenburg).

#168949 - $15.00 USD Received 21 May 2012; revised 6 Jul 2012; accepted 6 Jul 2012; published 1 Aug 2012